Chalcogenide Letters Vol. 16, No. 7, July 2019, p. 357 - 363

NANOSTRUCTURED POR Si-Cu_2ZnSnS_4 THIN FILMS

M. A. JAFAROV*, E. F. NASIROV, S. A. JAHANGIROVA, R. MAMMADOV
Baku State University, Baku, Azerbaijan

Nanostructure CZTS thin film was fabricated by electrodeposition technique. To manufacture the heterojunctions, p-type *c*-Si wafers of (100) orientation were used as a substrate. Before anodization, the surface of the *c*-Si substrates were etched in an aqueous solution of HF and further washed in distilled water (at temperature of 80°*C* and ethyl alcohol and then dried in air. The current-voltage characteristics of the CZTS /PS solar cell under dark conditions show that forward bias current variation approximately exponentially with voltage bias. The capacitance for Nano- CZTS /PS Solar Cell decreases with the increase of the reverse bias voltage and with the increasing of etching time of nPS layers. That heterojunctions demonstrate good photo-response in the wavelength range of 510 ÷ 650 *nm.*

(Received March 26, 2019; Accepted July 17, 2019)

Keywords: CZTS, Thin films, Electrochemical deposition, Current-voltage characteristics

1. Introduction

Compound semiconductors such as Cu_2ZnSnS_4 are important because of their photovoltaic, photoelectrochemical, and electroluminescent applications and, thus, they have much attention. Recently, there have been many efforts to produce nanosized materials, because electrical and optical properties can be varied via chemical control over the size, stoichiometry, and interparticle separation. These materials have been synthesized by various techniques including pyrolysis of organometallic compounds and sol gel synthesis. In recent years, there has been considerable interest of using thin films in solar cells [1-3]. Photoelectrical properties of these heterojunctions have found practical application in phototransistors and in solar cells. However, the physics and technology of heterojunctions have also other prominent aspect - creation, research and practical application of non-ideal heterojunctions. The big set of various effects and phenomena in non-ideal heterojunctions related to various properties of semiconductors on both junction regions of heterocontacts have been observed [4-6]. Perspectivity of practical application of the non-ideal heterojunctions is related first to more economic technology of creation of polycrystalline heterostructure in comparison with the monocrystalline [7-9].

Porous silicon has attracted great attention due to its room temperature photoluminescence in the visible light range. As we know that, the bulk crystalline silicon has an indirect gap at 1.1 eV at room temperature, which results in a very inefficient radiative recombination and produced light in the infrared region. Therefore, the strong visible light emission in porous silicon is quite surprising and such structure can exhibit a large variety of morphologies and particles sizes. Porous silicon shows different features in comparison to the bulk silicon such as shifting of fundamental absorption edge into the short wavelength and photoluminescence in the visible region of the spectrum. However, different hypothesis is reported on photoluminescence from porous silicon surface. Porous silicon consists of a network of nanoscale sized silicon wires and voids which formed when crystalline silicon wafers are etched electrochemically in hydrofluoric acid based electrolyte solution under constant anodization conditions. The precise control of porosity and thickness allows the tailoring of optical properties of porous silicon and has opened the door to a multitude of applications in optoelectronics technology [10-12]. Such structures

*Corresponding author: maarif.jafarov@mail.ru

consist of silicon particles in several nanometer size separated by voids. Hence, porous silicon layers are regarded as nanomaterials, which can be obtained by the electrochemical etching of silicon wafer. Porous silicon structures has good mechanical robustness, chemical stability and compatibility with existing silicon technology therefore has a wide area of potential applications such as waveguides, In section two, the synthesis and characterization of electrochemically anodized nanocrystalline porous silicon layers is done, then, the setup was used in fabrication as a device of Nano-CdS/PS heterojunction solar cell, and investigating the electrical properties of the heterojunction [13,14] . This paper is devoted to studying the ZnCdS/por-Si/p-Si heterostructure. ZnCdS films can be successfully used in the development of photoelectric solar energy converters with an absorbing layer based on silicon.

Despite rather great attention given to ZnCdS/por-Si/p-Si heterostructures, the current-f low mechanisms in them have not yet been adequately studied. At the same time, such studies are urgent, since the features of the current-f low mechanisms control the main characteristics of semiconductor devices to a large extent.

2. Experimental

CZTS thin films were electrodeposited potentiostatically on ITO and por.Si substrates supported by polyethylene terephthalate (PET). Before deposition, a substrate pre-treatment consisting in an ultrasonic degreasing in organic solvents (first step: acetone, second step: isopropilic alcohol, 15 min each step) was adopted, in order to obtain uniform deposits.

To manufacture the heterojunctions, p-type *c*-Si wafers (2.5 $Ohm \cdot cm$ resistivity and 0.2 ÷ 0.3 *mm* thickness) of (100) orientation were used as a substrate. Before anodization, the surface of the *c*-Si substrates were etched in an aqueous solution of HF and further washed in distilled water (at temperature of 80°*C*) and ethyl alcohol and then dried in air. The anodization of *c*-Si substrate surface was carried out in Teflon chamber with Pt cathode. HF: ethanol solution (1:1) were used for the porous silicon formation. The anodization voltage, current density and anodization time were 30*V*, 40-70 mA/cm^2 and 30–1800 *sec*, correspondingly. Depending on the anodization current and time porous-Si with porous size of 7 – 50 *nm* were prepared on the surface of *c*-Si.

Depositions were carried out potentiostatically under nitrogen atmosphere at room temperature from a de-aerated aqueous solution containing $CuSO_4$ (0.01M), $ZnCl_2$ (0.01M), $SnCl_4$ (0.02M) and $Na_2S_2O_3$ (0.2M). To optimize the stoichiometry of the deposit, electrochemical baths with different compositions, obtained mixing different volumes of the above-mentioned solutions, were tested. The final pH was about 5, it was obtained adding lactic acid and NaOH (10M). Electrodeposition was performed for 45 min, at a potential of -1.05V vs. saturated calomel electrode (SCE); electrochemical experiments were performed using a PAR potentiostat/galvanostat (model PARSTAT 2273). A standard three-electrodes cell was employed, with a platinum net as counter electrode and a SCE as reference.

Morphological analyses were performed by scanning electrode microscopy (SEM), using a FEI field-emission gun (FEG) environmental scanning electron microscope (model QUANTA 200F). In order to ensure the reliability of the different characterizations, these were performed on different pieces of the same sample. Films were also characterized by XRD analysis, using an ItalStructures (APD2000) diffractometer having the Cu Kα radiation (λ= 0.154nm) as the source, with a step of 0.02° and a measuring time of 0.5s for each step. The cell was equipped with flat quartz windows for allowing sample illumination, obtained using a 150W Xe lamp (Oriel) coupled to a UV/visible monochromator (Baush Lomb), mounted in an optical line with quartz optics. A computerized 619 Electrometer/Multimeter was used to measure the current-voltage (I-V) characteristics of the resulting solar cells using a solar simulator with light intensity corrected to a power density of 100 $mW \cdot cm^{-2}$ (AM1.5). The results of the materials characterisation and device assessment are presented and discussed in the next section.

3. Results and discussion

The morphology of PS was investigated using SEM (Fig. 1). SEM data indicate that the increase of anodization current density leads to the increase of the resulting pore size and a significant surface flattening between the pores.

In order to achieve a more direct insight into the surface structural features of the films, SEM imaging had been performed. SEM images of CZTS thin films deposited at potential of 0.86 *V* onto the *c*-Si/PS (with pores size of 10; 20 and 30 *nm*) are shown in Fig. 2.

The films deposited onto the substrates with pores size 10 *nm* shows micro-texture structure. The grain sizes were in the range from ∼20 to 70 μm. As seen from Fig. 2c, when Si with pores size of 10 *nm* is used as substrate, the size of the nano-grains gets reduced due to controlled process of nucleation and nano-size grains are uniformly distributed at the surface.

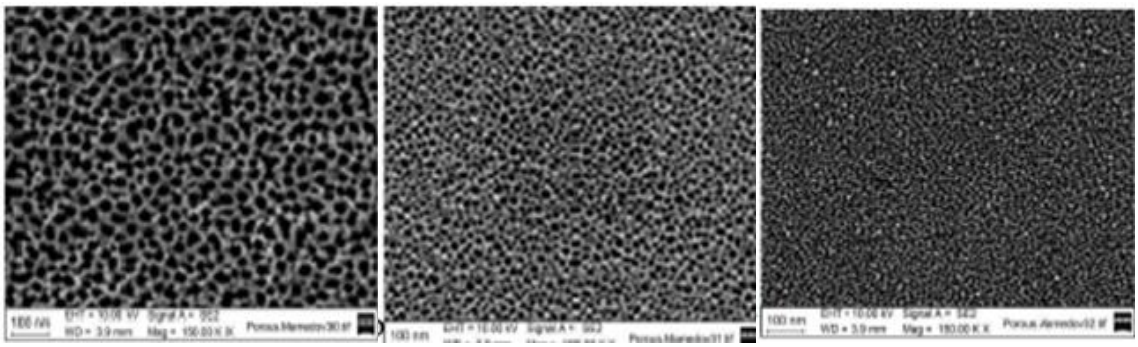

Fig. 1. SEM images of porous silicon prepared at different regimes of anodization: (a) 30V; 70 mA/cm^2; 1800 sec; (b) 30V; 55 mA/cm^2; 1800 sec; (c) 30 V; 40 mA/cm^2; 400 sec.

Size of particles, as determined by SEM, is found as 80-190 *nm*. As seen from SEM images, ZnCdS films shows nano-grain texture, with increasing the pores size from 10 to 30 *nm* (Figure 1 b) . The size of the grains was different from each other, indicating irregular growth rate of the grains. The pass direction corresponds to positive polarity of the external bias on the *c*-Si layers. Rectification increases from 180 up to 1100, with increasing the pores size from 10 to 20 *nm*. Further increase in pore sizes leads to sharp decrease of rectification (∼12÷15). It is assumed that the change in rectification factor value depending on the pore size is due to the oxygen or nitrogen molecules, because in order to remove excess water from pores and films, heterojunctions were dried in air, just after the deposition (as-deposited heterojunctions). As seen from figure, the size of crystallites of the CZTS films can be controlled by selecting the pores size of silicon.

Depending on composition of electrolytic bath used for the deposition process, it was possible to obtain different CZTS deposits, characterized by different chemical compositions. It was necessary to investigate different baths prior to find the best experimental conditions leading to CZTS films with suitable composition for solar cell applications. We have checked the influence of bath composition on the kinetics of deposition and on film morphology and composition, varying the volumes of mixed initial solutions. A compact enough CZTS layer covering uniformly all substrate area exposed to the solution was obtained. The as-deposited thin film was amorphous as revealed by X-ray diffraction pattern, that has not been reported here because practically flat. Thermal treatment would vary the structure of the film, but we didn't perform it because of ITO/PET substrate, which could not be exposed at high temperatures (PET decomposes at about 340°C). In fact, annealing would be efficient at temperatures higher than 400°C and, thus, it is necessary to change the substrate. Further investigations are in progress on other substrates in order to evidence a possible influence of thermal treatment on both crystallographic structure and chemical composition of the deposit.

The prefered orientation of the structure is in the <002> direction with the corresponding XRD peak at 2θ = 26.3°. However, the (002) peak was not used for estimating the crystallite size since it coincides with an İTO peak. As a result, the next higher peak which is the (101) peak at 2θ

~ 28.1° was used for this purpose. The estimated crystallite sizes using Scherrer equation were ~21 nm and 63 nm before and after annealing respectively. The d-spacing obtained for the annealed sample was 3.186 Å. The corresponding 2θ and d-spacing for the reference file are 28.2° and 3.164 Å respectively. Fig. 2 shows that the electrodeposited Cu_2ZnSnS_4 is highly oriented in the <111> direction with a cubic structure.

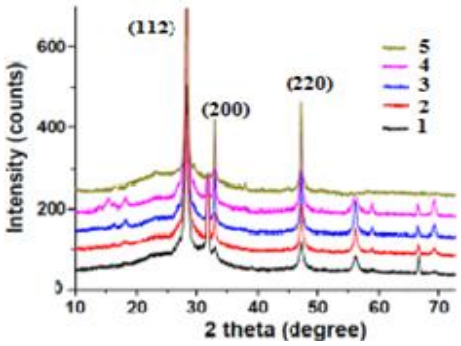

Fig. 2. X-ray diffraction patterns of electrodeposited polycrystalline Cu_2ZnSnS_4 highly oriented thin layers on glass/İTO (1) and Por-Si substrates (2,4-20 nm, 3,5-10 nm), befor (2,3) and after (4,5) heat treatment.

Atomic force microscopy (AFM) is one of the effective ways for the surface analysis of p-Si/10 *nm porous*-Si/ CZTS; thin films due to its high resolution and powerful analysis software (Fig. 2.).

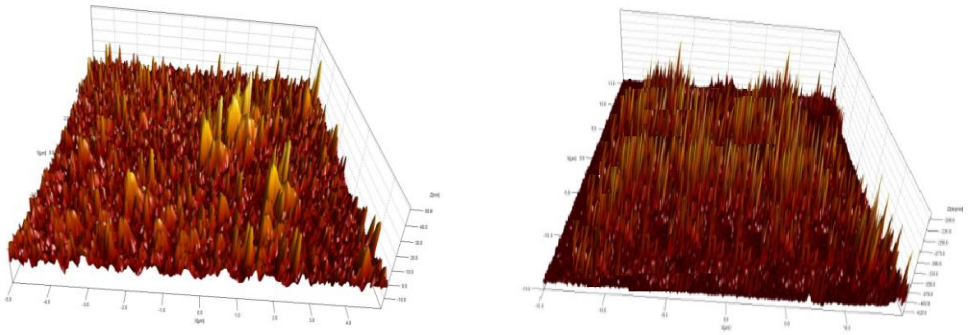

a) *b)*

Fig. 3. AFM images of electrdeposited films : (a) p-Si/20 nm porous-Si/ CZTS; (b) p-Si/10 nm porous-Si/ CZTS.

The current-voltage curves are the most commonly used characterization tool for the devices. In this technique, the current is measured as a function of voltage of the heterojunction, in both dark and light. Fig. 3 represents I-V characteristics under illumination with power intensities room temperature of the Nano- CZTS /PS heterojunction, containing nPS layers prepared at different etching times (10, 20 and 30) *min*. In general, the forward dark current is generated due to the flow of majority carriers and the applied voltage inject majority carriers which leads to decrease the value of built-in potential, and decrease the width of the depletion layer.

In this case, adsorbed oxygen or nitrogen molecules to the silicon pores creates the acceptor states in junction region and thus increase recombination acts. It is established that the degree of adsorption depends on pores size. To confirm this fact, heterojunctions were heated in vacuum at 50 -70°*C* and *J-V* characteristics were taken in vacuum. It is established that rectification in heterojunctions with pore size of 10 and 20 *nm* remained almost unchanged.

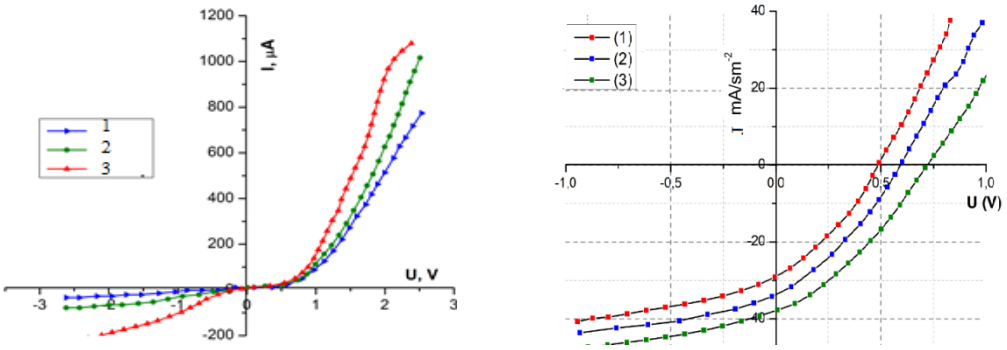

Fig. 4. I-V characteristics at dark and under illumination conditions at forward and reverse bias voltage for heterojunction Nano- CZTS /PS before (3-20nm,1-10nm) and after (2-10nm) HT.

Also, the reverse bias current contains two regions in the voltage region the current increases with increasing the applied voltage, and the generation current dominates. In addition, the current-voltage characteristics exhibit rectification behavior may be due to the hetrojunction potential barrier at the CZTS/PS interface.The rectification factor indicates the ratio between forward and reverse current at a certain applied bias voltage. Due to the high density of states of the nPS layer which will result in screening of internal field inside the nPS layer, this field would be nearly homogenously distributed through the nPS layer at higher voltages ($V > 1$ *V*), therefore, the forward bias characteristics will be controlled by the PSi layer resistance. This result explains the lowering of flow current in forward bias with the increasing of etching time of nPS layers, since the porosity of nPS layer increases with etching time and hence the resistance of nPS layer becomes too high which leads to low forward current. The photocurrent has been observed in reverse bias only, and we can see from this figure, that the presence of the light illumination strongly increases the reverse current. The photocurrent is always in the reverse bias direction due to it increases by increasing the depletion region width. The increasing of the reverse bias voltage leads to the increase in the internal electric field, which leads to an increasing in the probability of the separated electron-hole pairs.

The effect of preparation conditions of nPS layer such as etching time has very important effect on the photocurrent characteristics of the device, where one can observe from Figure 4, that the photocurrent is reduced with the increasing of etching time. This result can be explained since the porosity of nPS layer increases with the increasing of etching time. The increasing of porosity leads to increase the resistivity of nPS layer; therefore, the photocurrent will decrease.

The capacitance-voltage characteristics have been studied in this work. The variation of capacitance as a function of reverse bias voltage in the range of (0-1) *V* for Nano- CZTS/PS heterojunction, which prepared at different etching times (10, 20 and 30) *min* are shown in Figure 5. It is observed from this figure that the capacitance decreases with increasing the reverse bias. This decreasing was non-linear, that the capacitance becomes constant approximately at high voltages. This behavior is attributed to the increasing in the depletion region width which leading to the increasing of built-in voltage; it is obvious from this figure that the capacitance at zero bias voltage (Co) decreases with the increasing of etching time of nPS layers. This is attributed to the increase of porosity with the increasing of etching time, which leads to the increasing of the depletion region width and decreasing the capacitance.

The relation between inverse capacitance squared (C^{-2}) against the reverse bias at different values of etching time are shown in Figure 5. A linear relationship between C^{-2} and reverse bias voltage was obtained for the structure, this linear relationship represents that the junction was abrupt type. The interception of the straight line with voltage axis at ($1/C^2 = 0$), represents the built-in voltage. Assuming that the resulting junction is one-sided junction, these data were calculated according to Anderson model.

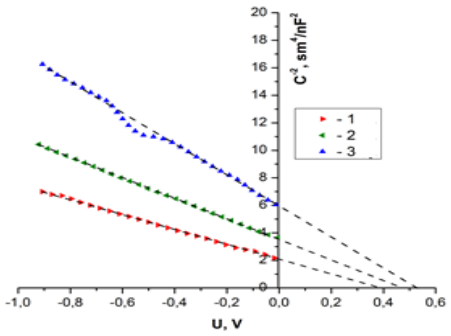

Fig. 5. The variation of $1/C^2$ as a function of reverse bias voltage for heterojunction Nano- CZTS /PS before (1) and after (2,3) HT at different etching times (2- 20 and 3-30) min.

In order to explain the reason of this, we investigated the spectral distribution of photocurrent (J_{ph}) depending on the pores size of silicon and morphology of ZnCdS films, in a wavelength range of 300÷1300 *nm* (Fig. 5). It is established that the profile of photocurrent spectrum depends on the pore size and morphology of CZTS films.

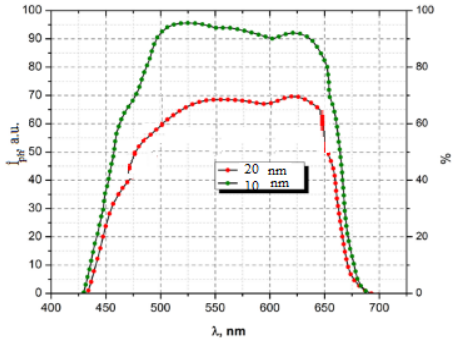

Fig. 6. Spectral distribution of photocurrent in heterojunctions depending on the pores size in Si.

Short wavelength peak for heterojunctions with a pore size of 7.4 *nm*, is observed at 640 *nm*, which corresponds to the band gap of CZTS films. The films deposited onto the silicon with pore size of 10 *nm* shows micro-structural morphology, as demonstrated by SEM images.

However, long-wavelength peak of spectrum at 1125 *nm* is due to the direct interband transitions in *c*-Si. It can be seen from Figure 6, that heterojunctions demonstrate good photo-response in the wavelength range of 510 ÷ 650 *nm*. It is assumed that this is due to light absorption in porous silicon. With increasing pores size until 10 *nm*, shift of peak at 640 *nm* to the short wavelength region of spectrum is observed, which associated by us with the nano-structural properties of CZTS films, i.e. band gap increasing with decrease of crystallite sizes in films. However, an increase of the optical path of light in nano-structured films leads to increase of degree of the light absorption, therefore, heterojunctions with pore sizes of 10 *nm*, shows greater efficiency compared heterojunctions with pore sizes of 7.4 *nm*.

4. Conclusions

Nanostructure CZTS thin film was fabricated by electrodeposition technique. To manufacture the heterojunctions, p-type *c*-Si wafers of (100) orientation were used as a substrate. Before anodization, the surface of the *c*-Si substrates were etched in an aqueous solution of HF

and further washed in distilled water (at temperature of 80°*C* and ethyl alcohol and then dried in air.

The current-voltage characteristics of the CZTS /PS solar cell under dark conditions show that forward bias current variation approximately exponentially with voltage bias. The capacitance for Nano- CZTS /PS Solar Cell decreases with the increase of the reverse bias voltage and with the increasing of etching time of nPS layers. That heterojunctions demonstrate good photo-response in the wavelength range of 510 ÷ 650 *nm.*

References

[1] D. Lincot, J. F. Guillemoles, S. Taunier, D. Guimard, J. Sicx-Kurdi, A. Chaumont, O. Roussel, O. Ramdani, C. Hubert, J. P. Fauvarque, N. Bodereau, Solar Energy 725 (2004).

[2] O. Bamiduro, G. Chennamadhava, R. Mundle, R. Konda, B. Robinson, M. Bahoura, Solar Energy 545 (2011).

[3] L. Ribeaucourt, G. Savidand, D. Lincot, E. Chassaing, Electrochimica Acta 6628 (2011).

[4] J. J. Scragg, P. J. Dale, L. M. Peter, G. Zoppi, I. Forbes, Physica Status Solidi (b)1772 (2008).

[5] H. Katagiri, K. Jimbo, S. Yamada, T. Kamimura, W. S. Maw, T. Fukano, T. Ito, T. Motohiro, Applied Physics Express 2008; 1: (article number 041201, 2 pages).

[6] K. Jimbo, R. Kimura, T. Kamimura, S. Yamada, W. S. Maw, H. Araki, K. Oishi, H. Katagiri, Thin Solid Films 5997 (2007).

[7] A. Weber, R. Mainz, T. Unold, S. Schorr, H. W. Schock, Physica Status Solidi (c) 1245 (2009).

[8] P. K. Sarswat, M. L. Free, Physica B **407**, 108 (2011).

[9] B. A. Schubert, I. M. Ko¨tschau, S. Cinque, H. W. Schock, G. Meran, Proceedings of the 23rd EU-PVSEC, Valencia, 3788 (2008).

[10] H. Mamedov, M. Muradov, Z. Konya, A. Kukovecz, K. Kordas, S. I. Shah, Photonics Letters of Poland **10**(3), 73.

[11] H. M. Mamedov, V. U. Mammadov, V. J. Mammadova, Kh. M. Ahmedova, J. Optoelectron. Adv. M. **20**(9-10), 468 (2018).

[12] V. V. Tregulov, V. G. Litvinov, A. V. Ermachikhin, Semiconductors **52**(7), 891 (2018).

[13] Y. B. Kumar, P. U. Bhaskar, G. S. Babu, V. S. Raja, Phys. Status Solidi A **207**, 149 (2010).

[14] Y. B. K. Kumar, G. S. Babu, P. U. Bhaskar, V. S. Raja, Physica Status Solidi A **207**, 149 (2009).